

University of Dundee

Limiting Extracellular Matrix Expansion in Diet-Induced Obese Mice Reduces Cardiac Insulin Resistance and Prevents Myocardial Remodelling

Musale, Vishal; Murdoch, Colin E.; Banah, Ayman K.; Hasib, Annie; Hennayake, Chandani K.; Dong, Bo

Published in:
Molecular Metabolism

DOI:
[10.1016/j.molmet.2024.101970](https://doi.org/10.1016/j.molmet.2024.101970)

Publication date:
2024

Licence:
CC BY

Document Version
Publisher's PDF, also known as Version of record

[Link to publication in Discovery Research Portal](#)

Citation for published version (APA):

Musale, V., Murdoch, C. E., Banah, A. K., Hasib, A., Hennayake, C. K., Dong, B., Lang, C. C., Wasserman, D. H., & Kang, L. (2024). Limiting Extracellular Matrix Expansion in Diet-Induced Obese Mice Reduces Cardiac Insulin Resistance and Prevents Myocardial Remodelling. *Molecular Metabolism*, 86, Article 101970. Advance online publication. <https://doi.org/10.1016/j.molmet.2024.101970>

General rights

Copyright and moral rights for the publications made accessible in Discovery Research Portal are retained by the authors and/or other copyright owners and it is a condition of accessing publications that users recognise and abide by the legal requirements associated with these rights.

Take down policy

If you believe that this document breaches copyright please contact us providing details, and we will remove access to the work immediately and investigate your claim.

Limiting extracellular matrix expansion in diet-induced obese mice reduces cardiac insulin resistance and prevents myocardial remodelling



Vishal Musale¹, Colin E. Murdoch¹, Ayman K. Banah¹, Annie Hasib¹, Chandani K. Hennayake¹, Bo Dong², Chim C. Lang³, David H. Wasserman⁴, Li Kang^{1,*}

ABSTRACT

Objective: Obesity increases deposition of extracellular matrix (ECM) components of cardiac tissue. Since obesity aggregates with insulin resistance and heart disease, it is imperative to determine whether the increased ECM deposition contributes to this disease cluster. The hypotheses tested in this study were that in cardiac tissue of obese mice i) increased deposition of ECM components (collagens and hyaluronan) contributes to cardiac insulin resistance and that a reduction in these components improves cardiac insulin action and ii) reducing excess collagens and hyaluronan mitigates obesity-associated cardiac dysfunction.

Methods: Genetic and pharmacological approaches that manipulated collagen and hyaluronan contents were employed in obese C57BL/6 mice fed a high fat (HF) diet. Cardiac insulin sensitivity was measured by hyperinsulinemic-euglycemic clamp and cardiac function was measured by pressure-volume loop analysis *in vivo*.

Results: We demonstrated a tight association between increased ECM deposition with cardiac insulin resistance. Increased collagen deposition by genetic deletion of matrix metalloproteinase 9 (MMP9) exacerbated cardiac insulin resistance and pirfenidone, a clinically available anti-fibrotic medication which inhibits collagen expression, improved cardiac insulin resistance in obese mice. Furthermore, decreased hyaluronan deposition by treatment with PEGylated human recombinant hyaluronidase PH20 (PEGPH20) improved cardiac insulin resistance in obese mice. These relationships corresponded to functional changes in the heart. Both PEGPH20 and pirfenidone treatment in obese mice ameliorated HF diet-induced abnormal myocardial remodelling.

Conclusion: Our results provide important new insights into the role of ECM deposition in the pathogenesis of cardiac insulin resistance and associated dysfunction in obesity of distinct mouse models. These findings support the novel therapeutic potential of targeting early cardiac ECM abnormalities in the prevention and treatment of obesity-related cardiovascular complications.

© 2024 The Author(s). Published by Elsevier GmbH. This is an open access article under the CC BY license (<http://creativecommons.org/licenses/by/4.0/>).

Keywords Cardiac insulin resistance; Obesity; Extracellular matrix remodelling; Cardiac dysfunction

1. INTRODUCTION

Insulin resistance associated with increasing prevalence of obesity, is defined as the inability of insulin to activate insulin signalling to effectively regulate multiple cellular processes including the promotion of glucose uptake and utilisation as fuels in the heart [1]. Importantly, cardiac insulin resistance contributes to myocardial dysfunction [2]. This is mediated by myocardial metabolic inflexibility, impaired calcium handling, mitochondrial dysfunction, dysregulated myocardial–endothelial interactions resulting in energy deficiency, impaired diastolic function, and myocardial cell death [3]. Although factors including oxidative stress, altered secretion of adipokines/cytokines, and neurohormonal activation in the renin-angiotensin system have

been proposed to contribute to cardiac insulin resistance [1–3], the primary mechanisms underlying insulin resistance in the cardiovascular system are still not fully defined.

We have previously reported *in vivo* evidence that demonstrated increased expression of extracellular matrix (ECM) components contributed to the pathogenesis of obesity-associated insulin resistance in skeletal muscle [4,5], liver [6], and adipose tissue [7]. Even though the heart is central to many obesity-associated disease states, maladaptive ECM remodelling in obesity-associated cardiac insulin resistance and related cardiac dysfunction has received little attention. The heart ECM comprises a complex network of macromolecules including proteins, proteoglycans, and growth factors, which provide structural and biochemical support to the surrounding cells and are essential for

¹Division of Cellular and Systems Medicine, School of Medicine, University of Dundee, Dundee, Scotland, UK ²Department of Cardiology, Shandong Provincial Hospital Affiliated to Shandong University, Shandong, Jinan, China ³Division of Molecular and Clinical Medicine, School of Medicine, University of Dundee, Dundee, Scotland, UK ⁴Department of Molecular Physiology and Biophysics, Mouse Metabolic Phenotyping Center, Vanderbilt University, Nashville, TN, USA

*Corresponding author. Division of Cellular and Systems Medicine, JWCC, School of Medicine, University of Dundee, Dundee DD1 9SY, UK. E-mail: l.kang@dundee.ac.uk (L. Kang).

✉ (L. Kang)

Received March 17, 2024 • Revision received May 16, 2024 • Accepted June 14, 2024 • Available online 20 June 2024

<https://doi.org/10.1016/j.molmet.2024.101970>

cellular and whole body homeostasis [8]. Myocardial fibrosis, characterised by excessive deposition of ECM components, leads to stiffening of the ventricles and negatively affects both contraction and relaxation of the heart [9]. Increased deposition of ECM components (e.g. collagens) has been shown to be key determinants of the increased left ventricular stiffness in patients with both heart failure with reduced ejection fraction and heart failure with preserved ejection fraction [10,11]. It is noteworthy that remodelling of the heart ECM to a profibrotic state can occur early and precede development of clinical fibrosis or cardiac histologic changes in hypertrophic cardiac conditions [11]. Therapies that can potentially inhibit the progression of these early changes of the ECM to severe fibrosis may also influence cardiac insulin resistance and preserve left ventricular function, thereby preventing the development of further cardiovascular complications.

In the present study the hypothesis that cardiac insulin resistance is associated with increased deposition of ECM components in the heart, leading to impaired cardiac function was tested. For this purpose, high fat (HF) diet fed, obese mouse models were studied. Further, we investigated whether pharmacological interventions that reduced heart ECM constituents using clinical and pre-clinical anti-fibrotic agents could reverse cardiac insulin resistance and improve cardiac function in obesity.

2. MATERIAL AND METHODS

2.1. Mouse models and treatment regimens

All animal experiments complied with the ARRIVAL guidelines and were carried out in compliance with the UK Animals (Scientific Procedures) Act 1986 and approved by the Animal Care and Use Committees of University of Dundee and Vanderbilt University. All procedures conformed to the guidelines from Directive 2010/63/EU of the European Parliament on the protection of animals used for scientific purposes or the NIH Guide for the Care and Use of Laboratory Animals. All the mice were maintained in an air-conditioned room (22 ± 2 °C) with a 12:12-h light–dark cycle. Standard laboratory chow (13% calories as fat, LabDiet 5001) and tap water were supplied *ad libitum*, unless dietary or pharmacological interventions indicated otherwise. Only male mice were studied due to their robust response to high fat (HF) diet-induced obesity and insulin resistance, therefore the current study may limit its clinical relevance to the male gender. Because animals underwent multiple terminal *in vivo* procedures (e.g. the hyperinsulinaemic-euglycaemic clamp and pressure-volume loop analysis), the number of animals used in each protocol varied due to different attrition rates and data variations. Sample size was determined by previous data using the same technique in the same laboratory. Detailed sample size for each measurement was indicated in corresponding figure/table legends.

2.1.1. High fat (HF) diet-induced obesity

Male C57BL/6J mice were purchased from the Jackson Laboratory. Following one week acclimatization period, mice starting from the age of 7 weeks were fed a HF diet (60% calories as fat, SDS 824054 or BioServ F3282) for 16 weeks to induce obesity or maintained on chow diet and used as lean controls.

2.1.2. MMP9 knockout mice

The homozygous matrix metalloproteinases 9 (MMP9) null mice (*mmp9*^{-/-}; Jackson Laboratory 007084) and their wild-type littermate controls (*mmp9*^{+/+}) on a C57BL/6J background were fed a HF diet (60% calories as fat, BioServ F3282) starting at 3 weeks of age for 16 weeks. All mice were studied at 19 weeks of age. Cardiac insulin sensitivity was measured by hyperinsulinaemic-euglycaemic clamps [12].

2.1.3. PEGylated human recombinant hyaluronidase PH20 (PEGPH20) treatment

To investigate the cardiometabolic regulation of antifibrotic agents in obesity, after 12 weeks of HF diet feeding (60% calories as fat, SDS 824054) mice were treated with either vehicle (10 mmol/L histidine, 130 mmol/L NaCl at pH 6.5) or PEGPH20 (Provided under a Material Transfer Agreement with Halozyme Therapeutics, San Diego, CA) at 1 mg/kg through tail vein injections, once every 3 days for 24 days [13]. This PEGPH20 dose and treatment regimen have been previously shown to reduce hyaluronan in mice fed a HF diet to the levels seen in chow-fed lean mice. A PEGylated form of human recombinant PH20 was used due to its increased half-life [14]. Animals were maintained on HF diet during the treatment. Body weight was monitored at 3-day intervals. At the end of treatment, body composition was determined using EchoMRI (Echo Medical Systems, TX), cardiac insulin sensitivity was determined by hyperinsulinaemic-euglycaemic clamp [5], and left ventricular cardiac dynamics was determined by Pressure-Volume (PV) loop analysis (Transonic) using PV conductance catheter in closed chest preparation.

2.1.4. Pirfenidone intervention

After 12 weeks of HF diet feeding (60% calories as fat, SDS 824054), mice received twice-daily treatments of either vehicle (0.25% carboxymethyl cellulose) or pirfenidone (125 mg/kg body weight) by oral gavage for 21 days, while animals were maintained on the HF diet. After the treatment, insulin sensitivity was measured by hyperinsulinaemic-euglycaemic clamp or cardiac function was analysed by PV loop in separate subgroups.

2.2. Hyperinsulinaemic-euglycaemic clamp

Five to seven days prior to clamps, catheters were implanted in the carotid artery and jugular vein of mice for sampling and intravenous infusion, with the exception of mice used in the pirfenidone study, a jugular catheter was implanted for intravenous infusion and blood sampling was obtained from tail vein bleeding. For the vascular cannulation surgery, anaesthesia was induced with 3.5–4.5% isoflurane (volume/volume) by inhalation for 2mins, then maintained with 1.5–2% isoflurane by inhalation for 1–2hrs. For the clamp procedure, mice received constant infusion of insulin ($4\text{mU} \cdot \text{kg}^{-1} \cdot \text{min}^{-1}$) to achieve hyperinsulinaemia. Euglycaemia was maintained by assessing blood glucose every 10min and adjusting the glucose infusion rate (GIR) accordingly. Blood samples were taken at 80, 90, 100, 110, and 120min for the measurement of glucose rates of appearance (Ra) and disappearance (Rd) using a primed-infusion of [$3\text{-}^3\text{H}$]glucose. At $t = 100$ and 120min, plasma insulin concentrations were measured. At 120min, [^{14}C]2-deoxyglucose intravenous bolus was administered and blood samples were collected from 2 to 35min after injection for the measurement of glucose uptake in tissues including the left-ventricle of the heart. Mice were euthanised under Schedule 1 (CO₂ exposure) after the last blood sample and tissues were excised for analysis of tissue [^{14}C]2-deoxyglucose-phosphate, immunohistochemistry, Western blotting, and qRT-PCR.

2.2.1. Non-steady state calculation of glucose flux

Ra and Rd were calculated using non-steady-state equations [15]. The glucose metabolic index (Rg) was calculated for the measurement of tissue-specific glucose uptake as previously described [16].

$$Ra = \frac{I - Vd \cdot A \cdot \frac{dSA}{dt}}{SA} \quad Rd = Ra - Vd \cdot \frac{dA}{dt}$$

R_a, *R_d*: glucose appearance and disappearance rates ($\text{mg} \cdot \text{kg}^{-1} \cdot \text{min}^{-1}$); *I*: tracer infusion rate (dpm/min); *V_d*: volume distribution of glucose; *A*: concentration of glucose (mg/dL); *SA*: specific activity of glucose (dpm/mg); *t*: time (min). Endogenous glucose appearance rate (EndoRa) was calculated by subtracting the GIR from total *R_a*.

2.2.2. Glucose uptake (*R_g*) in tissues including the left ventricle of the heart was calculated as follows

$$R_g = \frac{[^{14}\text{C}]2\text{DGP in tissue}}{\text{AUC plasma } [^{14}\text{C}]2\text{DG}} \cdot \text{average glucose concentration}$$

[¹⁴C]-2DGP: ¹⁴C-2-Deoxyglucose phosphate; [¹⁴C]2DG: 2-Deoxyglucose; AUC: Area under the curve.

Plasma insulin concentration was measured by Ultra-Sensitive Rat Insulin ELISA Kit (90060, CrystalChem). Plasma non-esterified fatty acid (NEFA) levels were measured by colorimetric analysis (434–91795, 436–91995, 4270–77000, WAKO Diagnostics).

2.3. Pressure-volume (PV) loop analysis

The real-time cardiac function of experimental mice was evaluated by left ventricle PV loops using an admittance catheter (1.2F, Transonic) coupled to ADV500 data acquisition system (Transonic) visualised by LabChart (ADInstruments). Mice were anaesthetized with 2% isoflurane (volume/volume) by inhalation for 30mins and the body temperature of mice was monitored by a rectal thermometer probe throughout the procedure. The PV catheter equipped with both pressure and volume sensors was introduced into the aorta via the carotid artery to measure arterial pressure. The catheter was then advanced to the left ventricle to record pressure and volume signals, under basal and inferior vena cava (IVC) occlusion conditions as described previously [17]. IVC occlusion, a gold standard for load-independent measurements of contractility (end-systolic pressure-volume relationship (ESPVR)) and compliance (end-diastolic pressure-volume relationship (EDPVR)) was performed by obstructing the return flow of blood to the heart. The load-dependent and independent hemodynamic data obtained from the experimental mice were analysed using Lab Chart Pro 8 software (ADInstruments). After the experimental procedure, mice were euthanised by exsanguination under anaesthesia and tissues were excised for analysis of immunohistochemistry, Western blotting, and qRT-PCR.

2.4. Immunohistochemistry

Paraffin-embedded left ventricular tissues were cut into a 5–6 μm section using a microtome and mounted onto the staining slide. Hyaluronan, collagen, CD31, CD45, and α -SMA expressions were assessed using biotinylated hyaluronan-binding protein (AMS.HKD-BC41, AMS Biotechnology), Picosirius Red (Direct Red 80, Sigma 365548), anti-CD31 antibody (NBP1-49805, Novus Biologicals), anti-CD45 antibody (BD Bioscience 550539), or anti- α -SMA antibody (Cell Signalling 19245), respectively. Cardiomyocyte area and capillaries were co-stained with wheat-germ agglutinin (WGA, 2BSCIENTIFIC RL-1022-5) and isolectin B4 (Vector B-1205, 2BSCIENTIFIC B-1205-05). For the staining of hyaluronan, CD31, CD45 and α -SMA, slides were lightly counterstained with Mayer's hematoxylin. The specificity of hyaluronan staining was confirmed by treating the sample section with or without recombinant human hyaluronidase PH20. For CD31 staining, bowel samples were used as a positive control. Images (10–12 images per animal) were

captured by Axiovision microscope (Zeiss Axioscope, Germany) and quantified using Image J software. Hyaluronan and collagen content was measured as the percentage of total left ventricular area under polarized light. Capillary density was quantified as the number of capillaries (CD31-positive structures) per square millimetres. CD45 and α -SMA positive cells were counted as cells per square millimetres.

2.5. Western blotting

Left ventricles of mouse hearts were dissected and homogenized in lysis buffer containing protease and phosphatase inhibitors as previously described [7]. Protein concentrations were determined and 20–40 μg of protein per sample was loaded onto 4–12% SDS-PAGE gels for protein detection, using antibodies against CD44 (AF6127, 1:1,000; R&D Systems), RHAMM (87129, 1:1000, Cell Signalling), TGF- β (ab179695, 1:1000, Abcam), Phospho-Smad2 (Ser465/467)/Smad3 (Ser423/425) (8828, 1:1000, Cell signalling), Smad2/3 (3102, 1:1000, Cell signalling), VCAM-1 (AF643, 1:1000, R&D Systems), BNP (ab19645, 1:1000, Abcam), Phospho-p38 MAPK (Thr180/Tyr182) (9211, 1:1000, Cell signalling), p38 MAPK (9212, 1:1000, Cell signalling), Phospho-SAPK/JNK (Thr183/Tyr185) (9251, 1:1000, Cell signalling), JNK (9252, 1:1000, Cell signalling), pERK1/2 (4370, 1:1000, Cell signalling), ERK (4695, 1:1000, Cell signalling), α -SMA (19245, 1:1000, Cell signalling), pAKT (9271, 1:1000, Cell signalling), and AKT (9272, 1:1000, Cell signalling). GAPDH (5174, 1:1000, Cell signalling), beta-tubulin (ab6046, 1:1000, Abcam), and ponceau staining were used as loading controls.

2.6. Quantitative real-time PCR

Total RNA was extracted using TriPure isolation reagent and reversed transcribed into cDNA using SuperScript™ II Reverse Transcriptase (18064014, ThermoFisher). Quantitative real-time PCR was carried out to amplify genes of interest using the Veriti 96-well Thermal Cycler, ThermoFisher. Primer sequences can be found in [Supplemental Table 1](#). Data were normalized to 18S gene expression and analysed using the $2^{-\Delta\Delta\text{CT}}$ method.

2.7. Statistical analysis

Data are presented as mean \pm S.E.M. Statistical analysis was performed using unpaired Student t-test or either one-way or two-way ANOVA followed by the Tukey's method for multiple comparisons where appropriate. The significance level was set at $p < 0.05$.

3. RESULTS

3.1. Increased ECM deposition in the heart is associated with cardiac insulin resistance in obesity

Protein expression of collagen III and collagen IV, and hyaluronan content in the heart were increased (or tended to be increased) in HF-fed obese mice when compared to chow-fed mice ([Figure 1A–D](#)). HF diet feeding in mice induced cardiac insulin resistance as shown by decreased glucose uptake in the heart during an hyperinsulinaemic-euglycaemic clamp (insulin clamp) ([Figure 1E](#)) [13]. Genetic deletion of MMP9 increased protein expression of collagen III and tended to increase protein expression of collagen IV in HF-fed mice when compared with HF-fed wildtype controls ([Figure 1F–H](#)). Increased collagen deposition in the HF-fed *MMP9*^{−/−} mice was accompanied by exacerbated cardiac insulin resistance with decreased glucose uptake in heart during an insulin clamp ([Figure 1I](#)) [12]. In contrast, pharmacological treatment of PEGPH20 decreased hyaluronan content in the heart of HF-fed obese mice which was accompanied by improved cardiac insulin resistance as evidenced by increased cardiac glucose

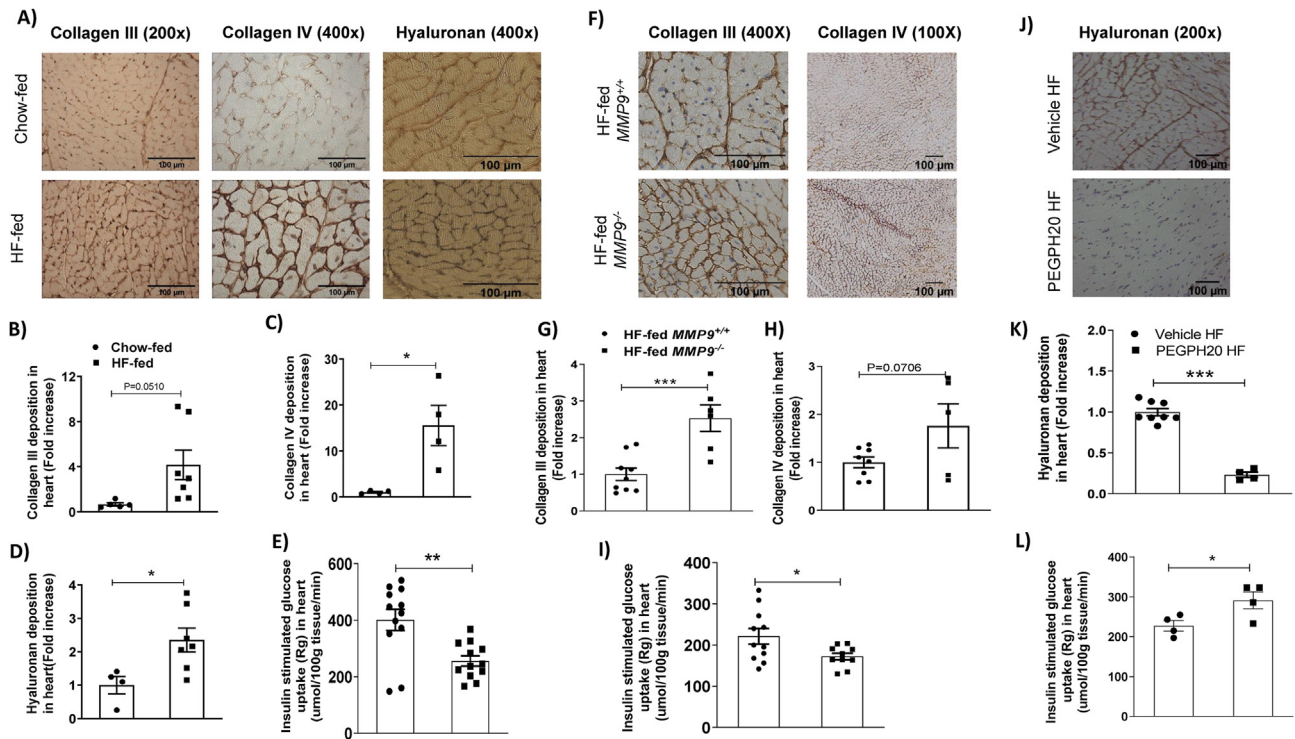


Figure 1: Increased deposition of ECM collagen and hyaluronan was associated with cardiac insulin resistance in obese mice. (A–D) C57BL/6 mice were fed either a chow diet or a 60% high fat (HF) diet for 16 weeks. Collagen III, collagen IV, and hyaluronan were detected by immunohistochemistry and quantified by ImageJ in heart sections. Representative images were shown. $N=4-5$ for chow-fed mice, and $n=4-7$ for HF-fed mice. (E) Cardiac insulin sensitivity was assessed by insulin-stimulated glucose uptake during a hyperinsulinemic-euglycemic clamp ($n=12$). (F–H) The homozygous MMP9 knockout mice ($MMP9^{-/-}$) and their wildtype littermate controls ($MMP9^{+/+}$) were fed with 60% HF diet for 16 weeks. Collagens III and IV were detected by immunohistochemistry and quantified by ImageJ in heart sections. $N=8-9$ for HF-fed $MMP9^{+/+}$, and $n=5-6$ for HF-fed $MMP9^{-/-}$. (I) Cardiac insulin sensitivity was assessed by insulin-stimulated glucose uptake during a hyperinsulinemic-euglycemic clamp ($n=11$). (J–K) C57BL/6 mice were fed a 60% HF diet for 12 weeks before receiving either vehicle or PEGPH20, once every 3 days for 24 days. Hyaluronan was detected by immunohistochemistry and quantified by ImageJ in heart sections. Representative images were shown. $N=8$ for Vehicle HF and $n=4$ for PEGPH20 HF. (L) Cardiac insulin sensitivity was assessed by insulin-stimulated glucose uptake during a hyperinsulinemic-euglycemic clamp ($n=4$). Unpaired student t-test was used for statistical analysis. * $p<0.05$, ** $p<0.01$, and *** $p<0.005$. Bar scale 100 μm

uptake during an insulin clamp (Figure 1J–L) [5]. These results suggest that obesity led to an increased ECM deposition in the heart which was tightly associated with cardiac insulin resistance in mice. Body weights of mice that were used in various study cohorts were exhibited in Supplemental Table 2.

3.2. Reduction of hyaluronan ameliorates obesity-associated cardiac dysfunction

To determine whether the association between increased ECM deposition and cardiac insulin resistance also extends to cardiac dysfunction in obesity, *in vivo* cardiac performance was measured in a separate group of mice fed with HF diet and treated with PEGPH20.

PEGPH20 treatment decreased total body mass and %fat mass but increased %lean mass in HF-fed obese mice (Supplemental Figs. 1A–B). Hyaluronan content in the heart was decreased by PEGPH20 (Supplemental Figs. 1C–D).

HF diet feeding in mice led to cardiac dysfunction (Figure 2 and Table 1). Systolic, diastolic and pulse pressures were increased in HF-fed vehicle-treated (HF-Vehicle) mice when compared with lean control mice. End systolic pressure (Pes) was significantly elevated, and there was a tendency albeit not significant ($p = 0.07$) for elevation of end diastolic pressure (Ped) after HF diet. Interestingly, the HF diet induced an inotropic effect in the left ventricle, with significantly higher dP/dt (max and min) and a tendency for an increase in a load-independent

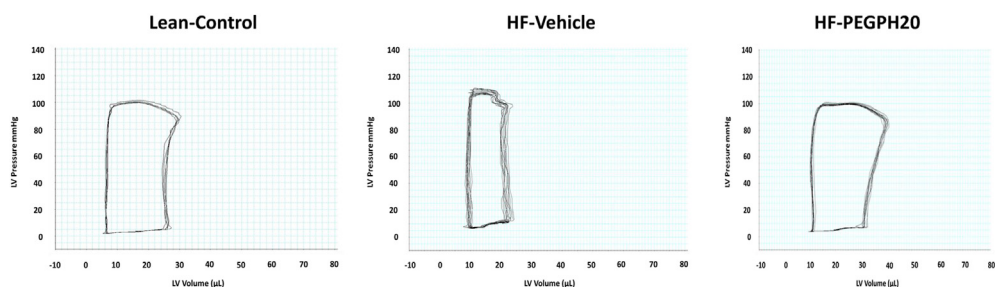


Figure 2: Representative left ventricle pressure-volume loops measured using admittance catheter in the experimental mice. HF-Vehicle mice had taller and narrower loops, showing higher pressures (Pes) and lower volumes (Ved and SV). PEGPH20 treatment reversed these cardiac changes.

Table 1 — Hemodynamic parameters from the pressure-volume loop analyses of chow-fed lean control mice and high fat (HF)-fed mice receiving vehicle or PEGPH20. N = 7 for Lean-Control, n = 10 for HF-Vehicle, and n = 11 for HF-PEGPH20. One-way ANOVA was used for statistical analysis. * $p < 0.05$, ** $p < 0.01$, *** $p < 0.001$ compared with Lean-Control; $\Delta p < 0.05$, $\Delta\Delta p < 0.01$ compared with HF-Vehicle; # $p = 0.07$ compared with Lean-Control. IVC: inferior vena cava occlusion; ESPVR: end systolic pressure volume relationship; EDPVR: end diastolic pressure volume relationship; VAC: ventricular-arterial coupling; LV: left ventricle.

Parameters	Lean-Control	HF-Vehicle	HF-PEGPH20
Blood Pressures			
Systolic blood pressure (mmHg)	97.04 ± 2.68	112.4 ± 3.53 **	98.45 ± 2.81 $\Delta\Delta$
Diastolic blood pressure (mmHg)	68.12 ± 1.19	77.70 ± 2.26 **	67.06 ± 2.63 $\Delta\Delta$
Pulse pressure (mmHg)	30.27 ± 0.59	37.35 ± 2.15 **	31.57 ± 0.38 $\Delta\Delta$
Baseline Parameters			
Heart rate	554.7 ± 7.81	545.5 ± 8.43	559.9 ± 11.37
End systolic volume (Ves) (μ L)	16.68 ± 1.80	13.38 ± 2.30	17.63 ± 3.60
End diastolic volume (Ved) (μ L)	29.41 ± 2.31	23.46 ± 2.49	32.36 ± 2.33 Δ
End systolic pressure (Pes) (mmHg)	92.53 ± 2.69	113.4 ± 3.89 ***	94.74 ± 2.97 $\Delta\Delta$
End diastolic pressure (Ped) (mmHg)	6.718 ± 1.08	10.90 ± 1.35 [#]	6.489 ± 1.22 Δ
Stroke volume (SV) (μ L)	22.03 ± 1.63	16.25 ± 1.46	23.59 ± 2.51 Δ
Ejection Fraction (EF) (%)	60.91 ± 3.23	55.23 ± 3.82	62.08 ± 4.54
Cardiac output (CO) (μ L/min)	12250 ± 890.9	8799 ± 713.6	13170 ± 1392 Δ
Stroke work (SW) (mmHg* μ L)	1953 ± 130.9	1644 ± 131.5	2136 ± 222.6
dP/dt max (mmHg/s)	8196 ± 580.1	10470 ± 348.4 *	8895 ± 224.5 Δ
dP/dt min (mmHg/s)	8083 ± 400.5	10360 ± 650.7 **	8045 ± 258.8 $\Delta\Delta$
Tau (ms)	5.794 ± 0.31	6.528 ± 0.36	5.961 ± 0.34
IVC			
ESPVR	4.138 ± 0.31	5.746 ± 0.44 [#]	4.158 ± 0.44
EDPVR	0.06494 ± 0.01	0.06211 ± 0.01	0.05274 ± 0.01
VAC			
Arterial elastance (Ea)	4.286 ± 0.39	6.303 ± 0.45 *	4.502 ± 0.45 Δ
End systolic elastance (Ees)	5.385 ± 0.53	8.977 ± 1.26	7.186 ± 1.04
VAC index	1.081 ± 0.18	0.9814 ± 0.14	0.6301 ± 0.07
Clinical Parameters			
Heart weight/Femur (mg/mm)	9.76 ± 0.85	11.16 ± 0.64	10.01 ± 0.37
LV/Femur (mg/mm)	7.83 ± 0.74	8.02 ± 0.55	7.83 ± 0.29

measurement of contractility (end systolic pressure-volume relationship (ESPVR), $p = 0.07$). The arterial elastance (Ea) was also increased in HF-Vehicle mice in comparison with the lean controls, implying an impaired ventricular arterial coupling. Taken together, mice fed a HF diet underwent abnormal myocardial remodelling, working under higher pressures (Pes) with an increased afterload (Ea) and an increased inotropic response (dP/dt and ESPVR). Diastolic function was not significantly altered by HF diet with the relaxation constant (Tau) and end diastolic pressure-volume relationship (EDPVR) remaining similar between HF-Vehicle and lean control mice.

Mice fed a HF diet for 12 weeks were administered PEGPH20 for 24 days while remaining on HF diet. PEGPH20 intervention prevented diet-induced myocardial remodelling (Figure 2 and Table 1). HF diet-induced increases in systolic, diastolic, and pulse pressures were eliminated by PEGPH20 treatment. PEGPH20 decreased Pes and Ped, increased end diastolic volume (Ved), stroke volume (SV) and cardiac output (CO). PEGPH20 corrected the HF diet-induced changes in dP/dt max, dP/dt min, ESPVR, and Ea. Other parameters such as heart rate, ejection fraction (EF), stroke work (SW), Tau, end systolic elastance (Ees), EDPVR, and ventricular arterial coupling index (VAC index) were not significantly different between groups. Neither HF diet feeding nor PEGPH20 treatment changed whole heart or left ventricle weights. These results suggest that PEGPH20 treatment prevented abnormal myocardial remodelling observed in mice after HF diet feeding.

3.3. Removal of hyaluronan reduces HF diet-induced cardiac hypertrophy, SMAD activation, and inflammation

HF diet feeding in mice increased both interstitial and perivascular collagen deposition in the left ventricle (Figure 3A–B). These increases were absent in PEGPH20-treated HF-fed (HF-PEGPH20) mice.

However, protein expression of α -SMA (smooth muscle actin), a marker of cardio-myofibroblast activation, was not different between mouse groups (Figure 3C). Concurrently, HF diet feeding in mice increased the cross-sectional area of cardiomyocytes, indicative of hypertrophy. This effect was partially restored by PEGPH20 treatment (Figure 3D–E). We also observed a notable decrease in both capillary density and the number of cardiomyocytes per mm^2 in HF-Vehicle mice compared with lean controls (Figure 3D, F–G). These decreases were not significantly changed by PEGPH20.

We further studied cellular signalling changes in the left ventricle associated with HF feeding and PEGPH20 treatment. Protein expression of CD44, one of the two primary hyaluronan receptors, was decreased in HF-Vehicle mice compared to lean controls. CD44 remained low in HF-PEGPH20 mice (Figure 4A–B). Protein expression of RHAMM, the other hyaluronan receptor was not changed in HF-Vehicle mice but was increased in HF-PEGPH20 mice relative to lean controls (Figure 4A,C). While TGF- β , total SMAD2/3, and phosphorylated SMAD2/3 were not different between groups, the ratio of pSMAD2/3 to total SMAD2/3 was significantly decreased in HF-PEGPH20 mice relative to HF-Vehicle mice, suggesting a decreased SMAD2/3 activation (Figure 4A, D–G). VCAM-1, vascular cell adhesion molecule 1, a marker of inflammation-associated vascular adhesion was increased by HF diet feeding. This effect of HF diet was reversed by PEGPH20 treatment (Figure 4A,H). BNP, brain natriuretic peptide, a biomarker of cardiac function was not different between groups (Figure 4A,I). MAPK signalling was not altered by HF feeding or PEGPH20 treatment independently. However, phosphorylated ERK1/2 and the ratio of pERK1/2 to total ERK1/2 were lower in HF-PEGPH20 mice relative to lean control mice (Supplemental Figure 2).

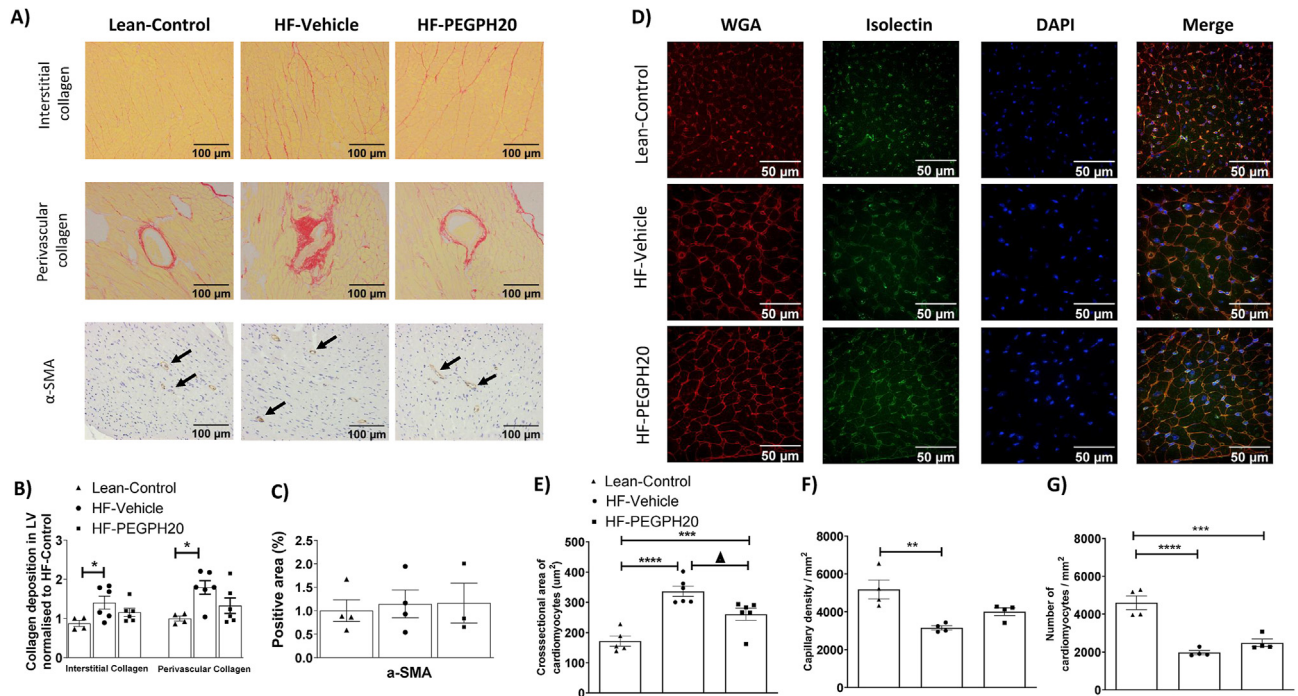


Figure 3: PEGPH20 treatment ameliorated high fat (HF) diet-induced myocardial fibrosis and hypertrophy. C57BL/6 mice were fed either a chow diet or a 60% HF diet for 16 weeks. After 12 weeks of HF feeding, HF-fed mice received either vehicle or PEGPH20, once every 3 days for 24 days. (A-C) Interstitial and perivascular collagens were detected by Sirius Red staining in left ventricle sections. Expression of α -SMA (smooth muscle actin) was detected by immunohistochemistry. Data were quantified by ImageJ. N=4-6. (D-G) Cardiomyocyte size was determined by Wheat Germ Agglutinin (WGA) staining. Capillary density was assessed by isolectin staining. DAPI was used to stain cell nuclei. Representative images were shown at 200x magnification for collagen deposition and α -SMA and 400x magnification for WGA & Isolectin images. Images were quantified by ImageJ. N=4-6. One-way ANOVA was used for statistical analysis. * $p < 0.05$, ** $p < 0.01$, *** $p < 0.005$, and **** $p < 0.001$ compared with Lean-Control; $\Delta p < 0.05$ compared with HF-Vehicle. Bar scale 100 and 50 μ m.

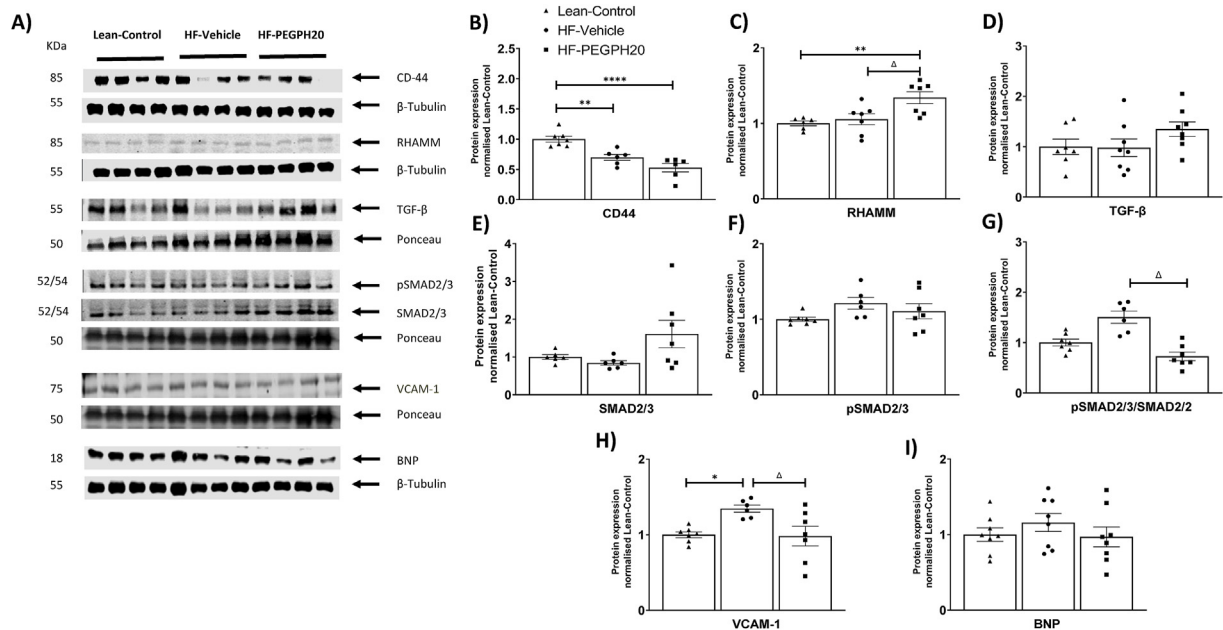


Figure 4: PEGPH20 treatment reduced SMAD2/3 activation and inflammation in the left ventricle of obese mice. C57BL/6 mice were fed either a chow diet or a 60% HF diet for 16 weeks. After 12 weeks of HF feeding, HF-fed mice received either vehicle or PEGPH20, once every 3 days for 24 days. Protein expression was determined by Western blotting. Representative blots were shown. N=6-8. One-way ANOVA was used for statistical analysis. * $p < 0.05$, ** $p < 0.01$, *** $p < 0.005$, and **** $p < 0.001$ compared with Lean-Control; $\Delta p < 0.05$ compared with HF-Vehicle. BNP: brain natriuretic peptide.

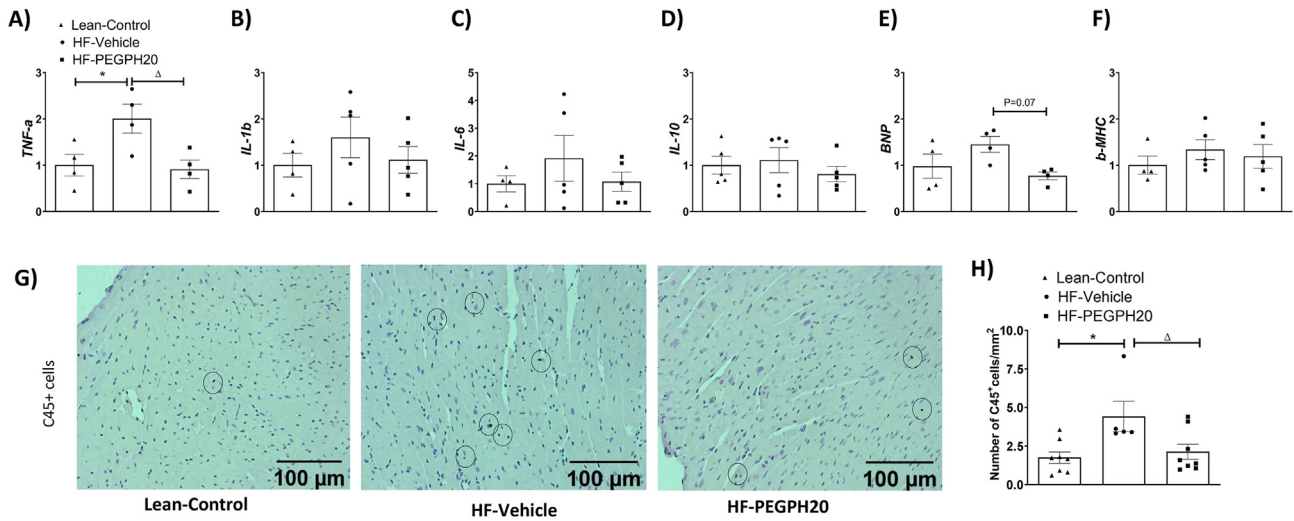


Figure 5: PEGPH20 treatment reduced high fat (HF) diet-induced inflammation in the left ventricle of obese mice. C57BL/6 mice were fed either a chow diet or a 60% HF diet for 16 weeks. After 12 weeks of HF feeding, HF-fed mice received either vehicle or PEGPH20, once every 3 days for 24 days. (A–F) mRNA expression was determined by qRT-PCR. $N = 4–5$. (G–H) CD45 positive cells were determined by CD45 immunohistochemistry and quantified by ImageJ. Representative images were shown at 200 \times magnification. $N = 5–8$. One-way ANOVA was used for statistical analysis. * $p < 0.05$ compared with Lean-Control; $\Delta p < 0.05$ compared with HF-Vehicle. BNP: brain natriuretic peptide; β -MHC: myosin heavy chain β . Bar scale 100 μ m.

HF diet feeding in mice increased cardiac inflammation as evidenced by increased gene expression of TNF- α and increased CD45⁺ cells in the left ventricle. The increase in inflammatory markers was prevented

by PEGPH20 treatment (Figure 5A, G–H). mRNA levels of IL-1 β , IL-6, IL-10, BNP and β -MHC were not significantly different between groups (Figure 5B–F).

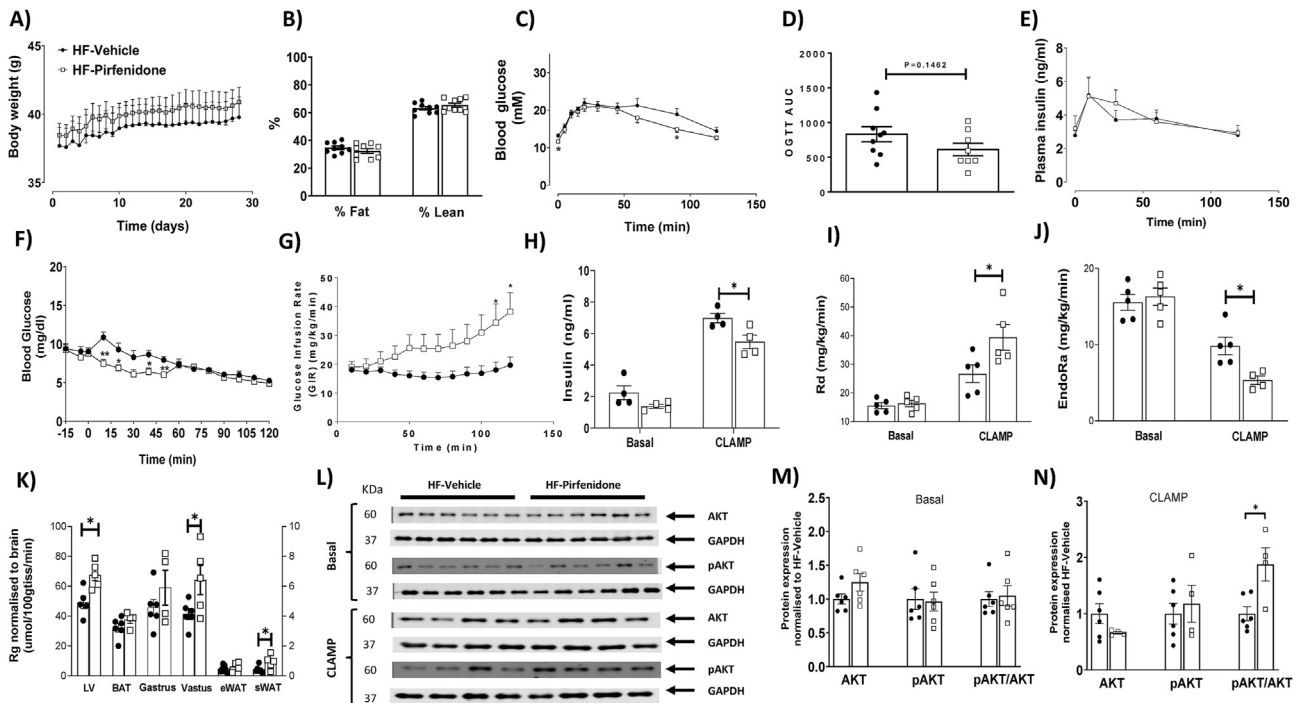


Figure 6: Pirfenidone improved cardiac as well as systemic insulin resistance in obese mice. C57BL/6 mice were fed with a 60% high fat (HF) diet for 16 weeks. After 12 weeks of HF feeding, mice received twice-daily treatments of vehicle or pirfenidone for 21 days. (A–B) Body weight was monitored daily and body composition was measured after the vehicle/drug treatment. $N = 9–10$. (C–E) Blood glucose, area under the curve of blood glucose, and plasma insulin were determined during an oral glucose tolerance test. $N = 8–10$. (F–K) Insulin sensitivity was determined by hyperinsulinemic-euglycemic clamps. (F) Blood glucose and (G) glucose infusion rate (GIR) were measured. $N = 5–6$. (H) Plasma insulin concentrations were measured at basal state as well as during the insulin clamp. $N = 4$. (I–J) Glucose disappearance (Rd) and endogenous glucose appearance (EndoRa) rates were measured during the clamp. $N = 4–5$. (K) Tissue-specific glucose uptake (Rg) was measured during the clamp $N = 4–6$. (L–N) Insulin signaling in the left ventricle was measured by pAKT/AKT ratio at both basal condition as well as post the insulin clamp, by Western blotting. Representative blots were shown and quantified. $N = 4–6$. Unpaired student t-test was used for statistical analysis for Panels D, K, M, and N, and two-way ANOVA followed by Tukey's method for multiple comparison was used for all the other panels. * $p < 0.05$.

3.4. Pirfenidone ameliorates cardiac insulin resistance in obese mice

In light of the increased collagen deposition in HF-fed mice, we tested whether pirfenidone, an anti-fibrotic drug which has been shown to decrease collagen deposition in the heart [18–21], has beneficial effects on cardiac insulin resistance and associated cardiac dysfunction in obese mice. Pirfenidone treatment did not change body weight or body composition of HF-fed obese mice (Figure 6A–B). During oral glucose tolerance tests, pirfenidone-treated HF-fed mice exhibited a modest improvement in glycaemic response compared to vehicle-treated HF-fed mice (Figure 6C). However, there was no difference in area under the glucose curve (AUC) or plasma insulin levels between the two groups (Figure 6D–E). During insulin clamps, the arterial glucose levels were clamped at 6.5 mmol/L at the steady state of the clamps (80–120 min) in all the mice (Figure 6F). Pirfenidone treatment increased glucose infusion rates (Figure 6G), but the clamp insulin was significantly lower in pirfenidone-treated mice than in vehicle-treated HF mice, indicating an improvement in insulin action in pirfenidone-treated mice (Figure 6H). Insulin increased the rate of glucose disappearance (Rd) and decreased the rate of endogenous glucose appearance (EndoRa) in all mice, but to a much greater extent in pirfenidone-treated mice compared to vehicle-treated mice (Figure 6I–J). In addition, Rg, a measure of tissue-specific glucose uptake was significantly higher in left ventricle, vastus lateralis muscle, and subcutaneous white adipose tissue of pirfenidone-treated mice than vehicle-treated mice (Figure 6K). Taken together, these results suggest that pirfenidone treatment improved systemic as well as cardiac insulin resistance in obese mice.

Consistent with increased cardiac insulin action, insulin signalling as determined as the ratio of pAKT/AKT was not changed at the basal state but was increased during insulin stimulation in the left ventricle of pirfenidone-treated mice relative to vehicle-treated mice (Figure 6M–N).

3.5. Pirfenidone modestly prevents HF diet-induced myocardial remodelling in obese mice, in association with decreases in collagen deposition, SMAD activation, MAPK activation, and cardiac inflammation

We next studied whether improved cardiac insulin resistance by pirfenidone was associated with reversal of obesity-associated abnormal myocardial remodelling. Pirfenidone decreased pulse pressure and dP/dt min, both of which were previously shown to be increased by HF diet in mice (Table 2). However, no other parameters were significantly changed by pirfenidone (Table 2). Heart weight and left ventricular weight also remained the same between pirfenidone and vehicle-treated mice (Table 2).

Interestingly, pirfenidone decreased interstitial, but not perivascular collagen deposition (Figure 7A–B). Protein expression of α -SMA, the cross-sectional area of cardiomyocytes, capillary density, and the number of cardiomyocytes per mm² were unchanged by pirfenidone (Figure 7C–G). Pirfenidone treatment decreased pSMAD2/3/SMAD2/3 ratio without affecting TGF- β expression (Figure 8A–C). Pirfenidone also did not affect α -SMA or VCAM-1 expression but decreased BNP expression by Western blotting (Figure 8A, D–F). In addition, pirfenidone treatment caused a significant decrease in total P38, a trend for a decrease in pP38, and a decrease in pJNK, without affecting ERK signalling (Figure 8A, G–I). Moreover, Pirfenidone decreased mRNA levels of TNF- α , IL-6, and BNP, without affecting mRNA levels of IL-1 β , IL-10 and β -MHC, or numbers of CD45⁺ cells (Figure 9A–H).

Table 2 — Hemodynamic parameters from the pressure-volume loop analyses of high fat (HF)-fed mice receiving vehicle or pirfenidone. N = 9 for HF-Vehicle, and n = 8 for HF-Pirfenidone. Unpaired student t-test was used for statistical analysis. ***p* < 0.01, ****p* < 0.005 compared with HF-Vehicle. IVC: inferior vena cava occlusion; ESPVR: end systolic pressure volume relationship; EDPVR: end diastolic pressure volume relationship; VAC: ventricular-arterial coupling; LV: left ventricle.

Parameters	HF-Vehicle	HF-Pirfenidone
Blood Pressures		
Systolic blood pressure (mmHg)	93.96 ± 2.64	91.87 ± 1.54
Diastolic blood pressure (mmHg)	60.53 ± 1.85	64.08 ± 1.34
Pulse pressure (mmHg)	32.76 ± 0.65	27.08 ± 0.97 ***
Baseline Parameters		
Heart rate	557.1 ± 8.89	568.0 ± 9.20
End systolic volume (Ves) (μL)	10.30 ± 1.88	15.14 ± 1.74
End diastolic volume (Ved) (μL)	28.14 ± 1.83	34.93 ± 3.48
End systolic pressure (Pes) (mmHg)	84.78 ± 4.28	88.76 ± 2.14
End diastolic pressure (Ped) (mmHg)	7.558 ± 0.79	8.070 ± 0.85
Stroke volume (SV) (μL)	20.43 ± 1.40	20.86 ± 1.99
Ejection Fraction (EF) (%)	71.90 ± 4.34	61.69 ± 2.16
Cardiac output (CO) (μL/min)	11410 ± 1053	11890 ± 1219
Stroke work (SW) (mmHg*μL)	1802 ± 103.5	1776 ± 166.2
dP/dt max (mmHg/s)	9887 ± 242.4	9515 ± 374.2
dP/dt min (mmHg/s)	9011 ± 216.4	7488 ± 463.4 **
Tau (ms)	5.851 ± 0.26	6.197 ± 0.30
IVC		
ESPVR	6.260 ± 0.93	5.468 ± 1.00
EDPVR	0.08802 ± 0.01	0.1091 ± 0.01
VAC		
Arterial elastance (Ea)	4.419 ± 0.44	4.331 ± 0.48
End systolic elastance (Ees)	9.179 ± 1.90	6.707 ± 0.99
VAC index	0.4918 ± 0.09	0.6840 ± 0.06
Clinical Parameter		
Heart weight/Femur (mg/mm)	10.71 ± 1.25	10.36 ± 0.48
LV/Femur (mg/mm)	7.32 ± 0.30	7.89 ± 0.24

4. DISCUSSION

Increased ECM deposition has been shown to contribute to obesity-associated insulin resistance in adipose tissue [22], skeletal muscle [4,5], and liver [6]. The present study demonstrates for the first time a tight association between collagen and hyaluronan deposition in the heart, cardiac insulin resistance, and associated abnormal myocardial remodelling in obese mice. We employed both genetic and pharmacological approaches to modulate ECM deposition in the heart of obese mice. By using these methodologies, we find that increased ECM collagens and hyaluronan in the heart lead to cardiac insulin resistance and cardiac dysfunction while reduction of this increase in ECM components ameliorates cardiac insulin resistance and preserves left ventricular performance in diet-induced obese mice. Glucose is a fuel for the heart particularly during stresses such as ischemia, increased workload, and hypertrophy due to pressure overload. The ability of insulin to promote glucose utilisation in cardiomyocytes directly impacts on cardiac function [2]. Our findings reveal the important niche extracellular components have in heart function. This study outlines a common sequelae that links cardiac fibrosis, insulin resistance, and dynamics. The results herein suggest a simplified therapeutic strategy whereby preventing the dysregulation of the cardiac ECM in obesity and pre-diabetes arrests the progression into cardiac dysfunction. We show a tight association between increased ECM deposition in the heart and cardiac insulin resistance in obesity, where increased collagen deposition by genetic deletion of MMP9 exacerbates cardiac insulin resistance and decreased hyaluronan deposition by PEGPH20

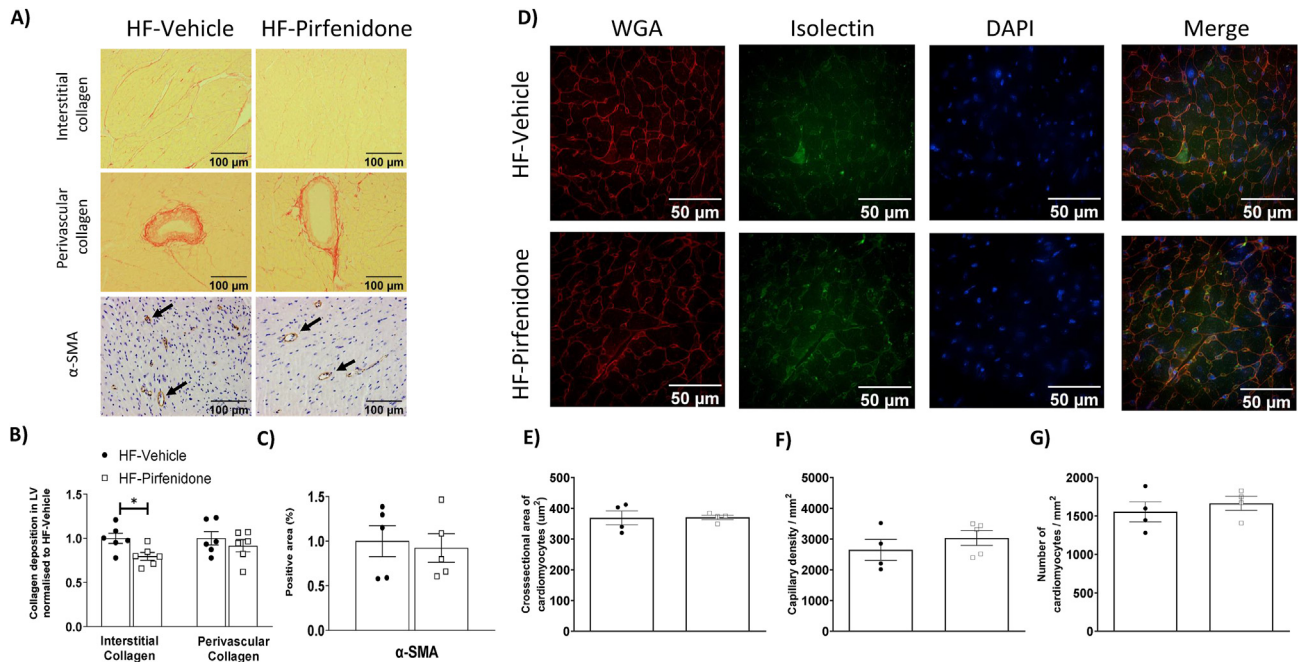


Figure 7: Pirfenidone reduced interstitial collagen deposition in the left ventricle of obese mice. C57BL/6 mice were fed with a 60% high fat (HF) diet for 16 weeks. After 12 weeks of HF feeding, mice received twice-daily treatments of vehicle or pirfenidone for 21 days. (A-C) Interstitial and perivascular collagens were detected by Sirius Red staining in left ventricle sections. Expression of α -SMA (smooth muscle actin) was detected by immunohistochemistry. Data were quantified by ImageJ. N=5-6. (D-G) Cardiomyocyte size was determined by Wheat Germ Agglutinin (WGA) staining. Capillary density was assessed by isolectin staining. DAPI was used to stain cell nuclei. N=4-5. Representative images shown at 200x magnification for collagen deposition and α -SMA and 400x magnification for WGA & isolectin images. Images were quantified by ImageJ. Unpaired student t-test was used for statistical analysis. * $p < 0.05$. Bar scale 100 and 50 μm .

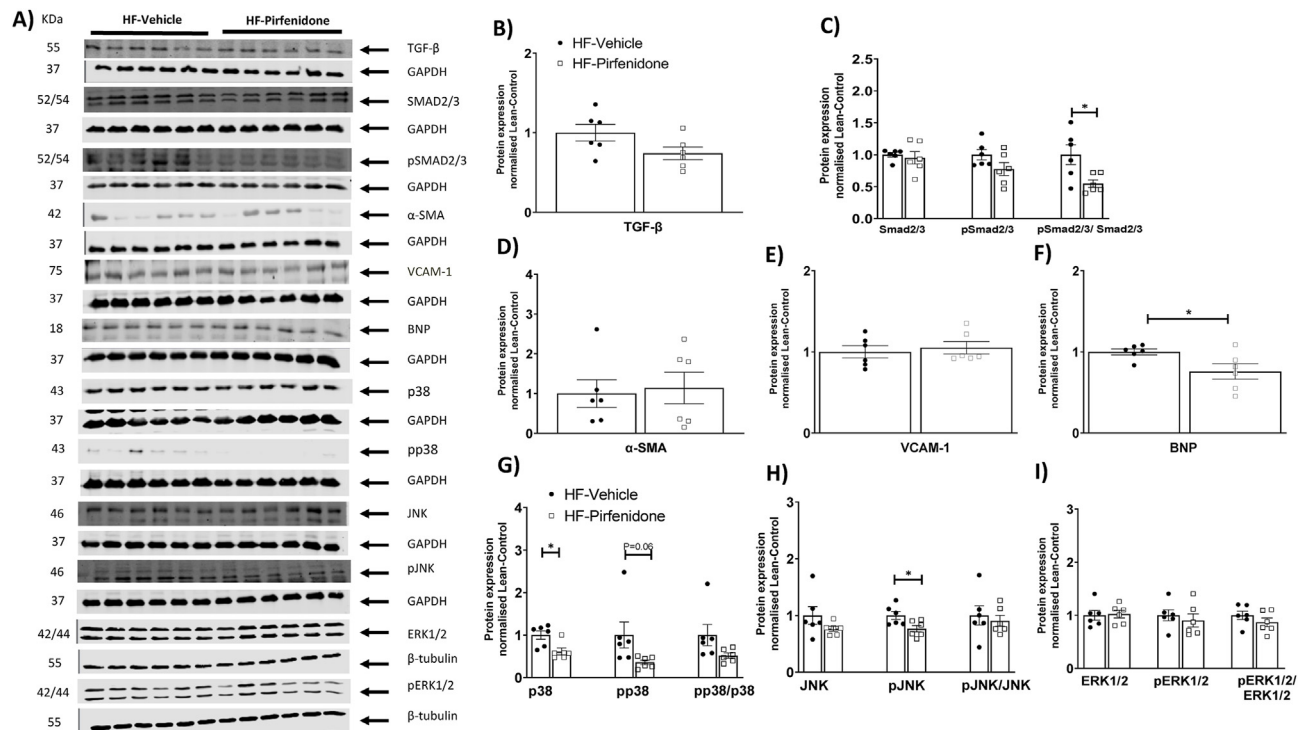


Figure 8: Pirfenidone reduced SMAD2/3 activation, brain natriuretic peptide (BNP) expression, and MAPK activation in the left ventricle of obese mice. C57BL/6 mice were fed with a 60% high fat (HF) diet for 16 weeks. After 12 weeks of HF feeding, mice received twice-daily treatments of vehicle or pirfenidone for 21 days. Protein expression was determined by Western blotting. Representative blots were shown. N=6. Unpaired student t-test was used for statistical analysis. * $p < 0.05$.

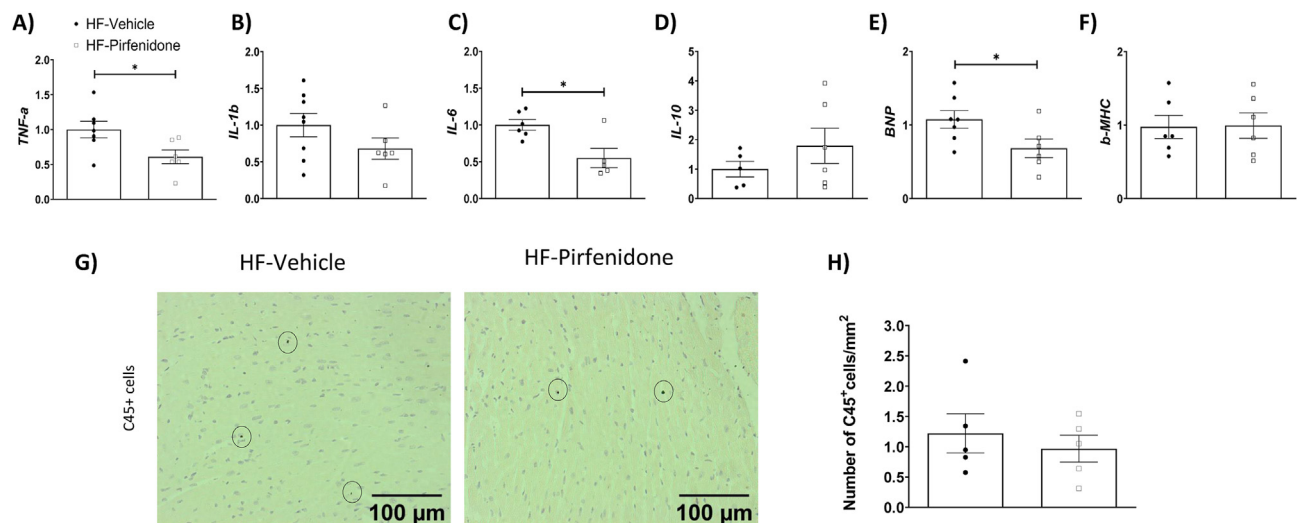


Figure 9: Pirfenidone decreased mRNA levels of pro-inflammatory markers TNF- α and IL-6, and a marker of cardiac function brain natriuretic peptide (BNP) in the left ventricle of obese mice. C57BL/6 mice were fed with a 60% high fat (HF) diet for 16 weeks. After 12 weeks of HF feeding, mice received twice-daily treatments of vehicle or pirfenidone for 21 days. (A-F) mRNA expression was determined by qRT-PCR. N=5-8. (G-H) CD45 positive cells were determined by CD45 immunohistochemistry and quantified by ImageJ. Representative images were shown at 200x magnification. N=5. Unpaired student t-test was used for statistical analysis. * $p < 0.05$. β -MHC: myosin heavy chain β . Bar scale 100 μ M.

treatment improves cardiac insulin resistance in obese mice. Using the hyperinsulinaemic-euglycaemic clamp, we measured insulin sensitivity in the heart of conscious mice *in vivo*. This technique overcomes drawbacks of other techniques such as glucose and insulin tolerance tests, which give measures of whole-body metabolism under non-steady state conditions [23]. Others have used *in vivo* PET-CT imaging to measure glucose uptake in the heart, yet these were not insulin-stimulated [24]. Our results are consistent with other studies that showed cardiac remodelling and interstitial fibrosis in obese rodents [25–27]. Here we show that modulation of ECM constitutes in the heart associates with myocardial responses to insulin. This is important as cardiac insulin resistance to glucose utilisation in cardiomyocytes contributes to cardiac dysfunction and the development of heart failure [1,28]. In a model of abdominal aortic constriction-induced cardiac hypertrophy where cardiomyocytes are enlarged, cardiac-specific insulin resistance is associated with left ventricular systolic and diastolic dysfunction, even in the absence of systemic insulin resistance [29].

The relationship between increased ECM deposition and cardiac insulin resistance extends to cardiac dysfunction. Using PV loop analyses, we show that in the setting of HF diet feeding, PV loops become narrower and taller (Figure 2), suggesting that the heart works with smaller volume (Ved, SV albeit insignificant) and higher pressures (Pes) because of increased afterload (Ea) and potentially preload (Ped). The heart adapts to the lower volume by increasing contractility (dP/dt, ESPVR) to maintain EF and CO. The enhanced contractility could be a result of increased stiffness due to increased ECM deposition and fibrosis, although diastolic function appeared to be unaffected (Tau, EDPVR). PEGPH20 treatment in HF-fed mice preserved both systolic and diastolic pressures and volumes, suggesting that PEGPH20 prevented changes in preload and afterload without the need to adapt for the maintenance of CO and SV. Previous studies using similar diet, 60% HF diet over 16 weeks, showed time-dependent increases in Tau, EDPVR and Ped, indicating diastolic dysfunction [30]. However, in our hands 16 weeks of HF diet did not initiate the same degree of cardiac changes. In the study by Tong et al. [30], mice that did not gain 20% of body weight after 2 months of HF diet consumption were excluded

from the analysis, whereas we included all experimental mice in our study. Therefore, we believe our data more accurately represent the heterogeneity of mouse's response to HF diet, enhancing its translatability to humans.

However, in people with obesity and Type 2 diabetes, a decrease in Ves and Ved has been recognised as markers of early diastolic dysfunction [31,32]. Despite not significant, we also observed a trend of decrease in Ves and Ved in HF-Vehicle mice relative to lean control mice, which was reversed in HF-PEGPH20 mice (Ved was indeed significantly increased in HF-PEGPH20 compared to HF-Vehicle mice). This same trend of increase in Ves and Ved was also observed in HF-Pirfenidone mice relative to HF-Vehicle mice albeit insignificant. These results suggest that our model also exhibited early signs of diastolic dysfunction, with increased duration of HF diet feeding which may lead to more prominent diastolic dysfunction.

Moreover, our mouse model of HF diet feeding exhibited an inotropic effect in the left ventricle, with significantly higher dP/dt (max and min) and a trend of increase in ESPVR. This enhanced contractility is uncommon in early reversible cardiomyopathy of HF-fed obese mice [30] or unexpected in clinical obesity cardiomyopathy [33]. However, our results were consistent with a previous study showing a compensatory increase in systolic function in women with moderate obesity [34].

Hyaluronan, a polysaccharide constituent of the ECM is associated with cardiac ECM remodelling and has been implicated in the cardiac defects of obesity [35]. Increased hyaluronan in the heart of hyaluronidase 2-deficient mice leads to cardiac fibrosis and impaired diastolic function [36]. Likewise, disruption of hyaluronan catabolism causes cardiac abnormalities in patients with a hyaluronidase 2 mutation [37]. Pharmacological removal of hyaluronan by PEGPH20 has been previously shown to improve muscle insulin resistance and reduce adipose tissue inflammation in obese mice [5]. Together with our findings in the heart, where it is shown to prevent HF diet-induced cardiac hypertrophy, fibrosis, and inflammation, we propose that hyaluronan is a promising target for obesity-related metabolic complications. PEGPH20 has been tested in patients with advanced cancers. Phase III trial of PEGPH20 in combination with the chemotherapies gemcitabine and

Nab-Paclitaxel in treating pancreatic cancer did not reach the primary outcome of improving overall survival for patients [38]. Several side effects of PEGPH20 including swelling in the hands and feet, muscle spasms, low white blood cell counts and muscle aches, have been reported. In mice, we have previously showed that PEGPH20 caused a transient weight loss and decrease in voluntary movement in a dose-dependent manner (0.001–10 mg/kg) [39]. At a dose of 1 mg/kg of PEGPH20 which was the dose used in the current study, these transient effects disappeared 3 days after the initial treatment commenced. CD44 and RHAMM are main cell surface receptors of hyaluronan that have been implicated in metabolic regulation and obesity [13,40,41]. Intriguingly, we observed that left ventricle CD44 was decreased in obesity and PEGPH20 caused an increase in RHAMM expression. The exact role of CD44 and RHAMM in regulating cardiac function and insulin resistance merit further investigations.

In addition to hyaluronan, increased collagen deposition is a characteristic of the hearts of obese individuals [42]. Pirfenidone is one of the two approved anti-fibrotic therapies for idiopathic pulmonary fibrosis, exerting its action through inhibiting collagen expression [18]. Although pirfenidone has been shown to reduce cardiac fibrosis and improve left ventricular function in pre-clinical models of myocardial infarction [20], its effect under obese condition had not been studied. Herein, we show that pirfenidone ameliorates cardiac as well as systemic insulin resistance in obese mice, which may contribute to its beneficial effects in cardiac function. A recent clinical trial has shown that pirfenidone reduces myocardial extracellular volumes in patients of heart failure with preserved ejection fraction [43], suggesting a high potential of repurposing pirfenidone for this condition. Our results provide further insight into the beneficial effects of pirfenidone on cardiac insulin resistance.

There is clinical evidence supporting our novel concept that ECM components may specifically drive metabolic and cardiac dysfunction in patients with cardiovascular conditions. Midwall fibrosis is an independent predictor of mortality in patients with moderate and severe aortic stenosis [44]. Excessive myocardial collagen cross-linking determined by the ratio of insoluble and soluble collagen is associated with hospitalisation for heart failure or cardiovascular death in patients with heart failure and arterial hypertension [45]. Moreover, a recent single-cell transcriptomic analysis reveals that fibroblast subtype changes and ECM remodelling highly correlate to disease progression at late stage of pathological cardiac hypertrophy [46]. Although these studies did not specifically examine patients with obesity, myocardial fibrosis and left ventricular hypertrophy are common features of subjects with abdominal obesity [47]. Therefore, myocardial fibrosis may provide a structural basis for pathological changes in the heart and ultimately account for the appearance of adverse cardiovascular events and outcomes [48].

The molecular pathophysiology of obesity-driven ECM remodelling or myocardial fibrosis is attributed to hypoxia, inflammation, activation of renin-angiotensin-aldosterone system, TGF- β signalling, and oxidative stress [35]. In the current study, we observed that HF diet feeding in mice induced inflammation (e.g. TNF- α , VCAM-1, CD45) and increased TGF- β -SMAD2/3 signalling in the left ventricle, contributing to the increased collagen and hyaluronan deposition. Treatment of PEGPH20 and pirfenidone reversed inflammation and SMAD2/3 activation. This could be due to a bidirectional regulation between inflammation and fibrosis [35]. Inflammation can trigger fibrosis by promoting TGF- β -SMAD2/3 activation and collagen deposition. Conversely, fibrosis can perpetuate inflammation by increasing tissue mechanical stress and

promoting hypoxia. Moreover, PEGPH20 and pirfenidone improved left ventricular function possibly through increasing myocardial insulin signalling (i.e. pAkt/Akt), without affecting the MAPK signalling pathways (i.e. pp38/p38, pJNK/JNK, or pERK/ERK1/2). Consequently, PEGPH20 and pirfenidone improved cardiac function, as evidenced by decreased protein or gene expression of BNP. Intriguingly, we observed that PEGPH20 caused a decrease in pERK1/2 and pERK/ERK1/2 ratio in the left ventricle of obese mice when compared to lean control mice, but not when compared to HF-Vehicle mice. These results suggest a diet–drug interaction which remains to be studied. In conclusion, our study establishes a novel link between increased ECM deposition, cardiac insulin resistance and cardiac dysfunction in obesity. By using two anti-fibrotic agents, which target two distinct ECM components, collagen and hyaluronan, our results show that reduction of ECM excess is sufficient to ameliorate cardiac insulin resistance and associated functional changes. These results highlight that early cardiac ECM remodelling in obesity-associated cardiac dysfunction can be mitigated and reversed. We propose that an intervention that prevents deleterious ECM expansion may be protective from further progression to severe cardiovascular consequences. It is, however, worth noting that only male mice were used in the current study, due to their robustness in HF diet-induced obesity and insulin resistance. Therefore, the applicability and transability of our findings to the female gender are limited and merit further investigations.

SOURCES OF FUNDING

This work was supported by Diabetes UK (15/0005256 and 21/0006329 to LK), British Heart Foundation (PG/18/56/33935 to LK), Tenovus Scotland (T18-23 to CM), National Natural Science Foundation of China (82070382 and 82371574 to BD), Taishan Scholars Programme (TS20190979 to BD), National Institute of Diabetes and Digestive and Kidney Diseases (DK050277, DK054902, and DK135073 to DHW). AB was supported by a PhD scholarship from Saudi Arabia Cultural Bureau.

CREDIT AUTHORSHIP CONTRIBUTION STATEMENT

Vishal Musale: Writing — original draft, Project administration, Methodology, Investigation, Formal analysis, Data curation, Conceptualization. **Colin E. Murdoch:** Writing — review & editing, Supervision, Methodology, Investigation, Formal analysis, Data curation. **Ayman K. Banah:** Writing — review & editing, Methodology, Investigation, Formal analysis, Data curation. **Annie Hasib:** Writing — review & editing, Methodology, Investigation, Formal analysis, Data curation. **Chandani K. Hennayake:** Writing — review & editing, Methodology, Investigation, Formal analysis, Data curation. **Bo Dong:** Writing — review & editing, Resources, Funding acquisition. **Chim C. Lang:** Writing — review & editing, Resources, Funding acquisition. **David H. Wasserman:** Writing — review & editing, Resources, Funding acquisition. **Li Kang:** Writing — original draft, Supervision, Resources, Project administration, Methodology, Funding acquisition, Conceptualization.

ACKNOWLEDGEMENT

PEGPH20 is an in-kind gift from Halozyme Therapeutics, Inc under a Material Transfer Agreement.

DECLARATION OF COMPETING INTEREST

The authors declare no conflicts of interests.

DATA AVAILABILITY

Data will be made available on request.

APPENDIX A. SUPPLEMENTARY DATA

Supplementary data to this article can be found online at <https://doi.org/10.1016/j.molmet.2024.101970>.

REFERENCES

- [1] Riehle C, Abel ED. Insulin signaling and heart failure. *Circ Res* 2016;118(7):1151–69.
- [2] Witteles RM, Fowler MB. Insulin-resistant cardiomyopathy clinical evidence, mechanisms, and treatment options. *J Am Coll Cardiol* 2008;51(2):93–102.
- [3] Aroor AR, Mandavia CH, Sowers JR. Insulin resistance and heart failure: molecular mechanisms. *Heart Fail Clin* 2012;8(4):609–17.
- [4] Kang L, Ayala JE, Lee-Young RS, Zhang Z, James FD, Neuffer PD, et al. Diet-induced muscle insulin resistance is associated with extracellular matrix remodeling and interaction with integrin alpha2beta1 in mice. *Diabetes* 2011;60(2):416–26.
- [5] Kang L, Lantier L, Kennedy A, Bonner JS, Mayes WH, Bracy DP, et al. Hyaluronan accumulates with high-fat feeding and contributes to insulin resistance. *Diabetes* 2013;62(6):1888–96.
- [6] Williams AS, Kang L, Zheng J, Grueter C, Bracy DP, James FD, et al. Integrin alpha1-null mice exhibit improved fatty liver when fed a high fat diet despite severe hepatic insulin resistance. *J Biol Chem* 2015;290(10):6546–57.
- [7] Bugler-Lamb AR, Hasib A, Weng X, Hennayake CK, Lin C, McCrimmon RJ, et al. Adipocyte integrin-linked kinase plays a key role in the development of diet-induced adipose insulin resistance in male mice. *Mol Metabol* 2021;49:101197.
- [8] Humphrey JD, Dufresne ER, Schwartz MA. Mechanotransduction and extracellular matrix homeostasis. *Nat Rev Mol Cell Biol* 2014;15(12):802–12.
- [9] Fan Z, Guan J. Antifibrotic therapies to control cardiac fibrosis. *Biomater Res* 2016;20:13.
- [10] van Heerebeek L, Hamdani N, Handoko ML, Falcao-Pires I, Musters RJ, Kupreishvili K, et al. Diastolic stiffness of the failing diabetic heart: importance of fibrosis, advanced glycation end products, and myocyte resting tension. *Circulation* 2008;117(1):43–51.
- [11] Ho CY, Lopez B, Coelho-Filho OR, Lakdawala NK, Cirino AL, Jarolim P, et al. Myocardial fibrosis as an early manifestation of hypertrophic cardiomyopathy. *N Engl J Med* 2010;363(6):552–63.
- [12] Kang L, Mayes WH, James FD, Bracy DP, Wasserman DH. Matrix metalloproteinase 9 opposes diet-induced muscle insulin resistance in mice. *Diabetologia* 2014;57(3):603–13.
- [13] Hasib A, Hennayake CK, Bracy DP, Bugler-Lamb AR, Lantier L, Khan F, et al. CD44 contributes to hyaluronan-mediated insulin resistance in skeletal muscle of high-fat-fed C57BL/6 mice. *Am J Physiol Endocrinol Metab* 2019;317(6):E973–83.
- [14] Thompson CB, Shepard HM, O'Connor PM, Kadhim S, Jiang P, Osgood RJ, et al. Enzymatic depletion of tumor hyaluronan induces antitumor responses in preclinical animal models. *Mol Cancer Therapeut* 2010;9(11):3052–64.
- [15] Steele R, Wall JS, De Bodo RC, Altszuler N. Measurement of size and turnover rate of body glucose pool by the isotope dilution method. *Am J Physiol* 1956;187(1):15–24.
- [16] Kraegen EW, James DE, Jenkins AB, Chisholm DJ. Dose-response curves for in vivo insulin sensitivity in individual tissues in rats. *Am J Physiol* 1985;248(3 Pt 1):E353–62.
- [17] Murdoch CE, Chaubey S, Zeng L, Yu B, Ivetic A, Walker SJ, et al. Endothelial NADPH oxidase-2 promotes interstitial cardiac fibrosis and diastolic dysfunction through proinflammatory effects and endothelial-mesenchymal transition. *J Am Coll Cardiol* 2014;63(24):2734–41.
- [18] Miric G, Dallemagne C, Endre Z, Margolin S, Taylor SM, Brown L. Reversal of cardiac and renal fibrosis by pirfenidone and spironolactone in streptozotocin-diabetic rats. *Br J Pharmacol* 2001;133(5):687–94.
- [19] Mirkovic S, Seymour AM, Fenning A, Strachan A, Margolin SB, Taylor SM, et al. Attenuation of cardiac fibrosis by pirfenidone and amiloride in DOCA-salt hypertensive rats. *Br J Pharmacol* 2002;135(4):961–8.
- [20] Nguyen DT, Ding C, Wilson E, Marcus GM, Olgin JE. Pirfenidone mitigates left ventricular fibrosis and dysfunction after myocardial infarction and reduces arrhythmias. *Heart Rhythm* 2010;7(10):1438–45.
- [21] Yamagami K, Oka T, Wang Q, Ishizu T, Lee JK, Miwa K, et al. Pirfenidone exhibits cardioprotective effects by regulating myocardial fibrosis and vascular permeability in pressure-overloaded hearts. *Am J Physiol Heart Circ Physiol* 2015;309(3):H512–22.
- [22] Weng X, Lin D, Huang J, Stimson RH, Wasserman DH, Kang L. Collagen 24 alpha1 is increased in insulin-resistant skeletal muscle and adipose tissue. *Int J Mol Sci* 2020;21(16).
- [23] Martins F, Campos DH, Pagan LU, Martinez PF, Okoshi K, Okoshi MP, et al. High-fat diet promotes cardiac remodeling in an experimental model of obesity. *Arq Bras Cardiol* 2015;105(5):479–86.
- [24] Jimenez-Gonzalez S, Marin-Royo G, Jurado-Lopez R, Bartolome MV, Romero-Miranda A, Luaces M, et al. The crosstalk between cardiac lipotoxicity and mitochondrial oxidative stress in the cardiac alterations in diet-induced obesity in rats. *Cells* 2020;9(2).
- [25] Wang HT, Liu CF, Tsai TH, Chen YL, Chang HW, Tsai CY, et al. Effect of obesity reduction on preservation of heart function and attenuation of left ventricular remodeling, oxidative stress and inflammation in obese mice. *J Transl Med* 2012;10:145.
- [26] Leopoldo AS, Sugizaki MM, Lima-Leopoldo AP, do Nascimento AF, Luvizotto Rde A, de Campos DH, et al. Cardiac remodeling in a rat model of diet-induced obesity. *Can J Cardiol* 2010;26(8):423–9.
- [27] Eid RA, Alkhateeb MA, El-Kott AF, Eleawa SM, Zaki MSA, Alaboodi SA, et al. A high-fat diet rich in corn oil induces cardiac fibrosis in rats by activating JAK2/STAT3 and subsequent activation of ANG II/TGF-1beta/Smad3 pathway: the role of ROS and IL-6 trans-signaling. *J Food Biochem* 2019;43(8):e12952.
- [28] Godsland IF, Lecamwasam K, Johnston DG. A systematic evaluation of the insulin resistance syndrome as an independent risk factor for cardiovascular disease mortality and derivation of a clinical index. *Metabolism* 2011;60(10):1442–8.
- [29] Zheng L, Li B, Lin S, Chen L, Li H. Role and mechanism of cardiac insulin resistance in occurrence of heart failure caused by myocardial hypertrophy. *Aging (Albany NY)* 2019;11(16):6584–90.
- [30] Tong M, Saito T, Zhai P, Oka SI, Mizushima W, Nakamura M, et al. Mitophagy is essential for maintaining cardiac function during high fat diet-induced diabetic cardiomyopathy. *Circ Res* 2019;124(9):1360–71.
- [31] Brady EM, Gulsin GS, Mirkes EM, Parke K, Kanagala P, Ng LL, et al. Fibro-inflammatory recovery and type 2 diabetes remission following a low calorie diet but not exercise training: a secondary analysis of the DIASTOLIC randomised controlled trial. *Diabet Med* 2022;39(8):e14884.
- [32] Gulsin GS, Brady E, Marsh AM, Squire G, Htike ZZ, Wilmot EG, et al. Clinical associations with stage B heart failure in adults with type 2 diabetes. *Ther Adv Endocrinol Metab* 2021;12:20420188211030144.
- [33] Ren J, Wu NN, Wang S, Sowers JR, Zhang Y. Obesity cardiomyopathy: evidence, mechanisms, and therapeutic implications. *Physiol Rev* 2021;101(4):1745–807.

- [34] Pascual M, Pascual DA, Soria F, Vicente T, Hernandez AM, Tebar FJ, et al. Effects of isolated obesity on systolic and diastolic left ventricular function. *Heart* 2003;89(10):1152–6.
- [35] Musale V, Wasserman DH, Kang L. Extracellular matrix remodelling in obesity and metabolic disorders. *Life Metab* 2023;2(4).
- [36] Chowdhury B, Xiang B, Liu M, Hemming R, Dolinsky VW, Triggs-Raine B. Hyaluronidase 2 deficiency causes increased mesenchymal cells, congenital heart defects, and heart failure. *Circ Cardiovasc Genet* 2017;10(1):e001598.
- [37] Muggenthaler MM, Chowdhury B, Hasan SN, Cross HE, Mark B, Harlalka GV, et al. Mutations in *HYAL2*, encoding hyaluronidase 2, cause a syndrome of orofacial clefting and cor triatriatum sinister in humans and mice. *PLoS Genet* 2017;13(1):e1006470.
- [38] Van Cutsem E, Tempero MA, Sigal D, Oh DY, Fazio N, Macarulla T, et al. Randomized phase III trial of pegvorhyaluronidase alfa with Nab-paclitaxel plus gemcitabine for patients with hyaluronan-high metastatic pancreatic adenocarcinoma. *J Clin Oncol* 2020;38(27):3185–94.
- [39] Kang L, Lantier L, Kennedy A, Bonner JS, Mayes WH, Bracy DP, et al. Hyaluronan accumulates with high-fat feeding and contributes to insulin resistance. *Diabetes* 2013;62(6):1888–96.
- [40] Weng X, Maxwell-Warburton S, Hasib A, Ma L, Kang L. The membrane receptor CD44: novel insights into metabolism. *Trends Endocrinol Metabol* 2022;33(5):318–32.
- [41] Bahrami SB, Tolg C, Peart T, Symonette C, Veisoh M, Umoh JU, et al. Receptor for hyaluronan mediated motility (RHAMM/HMMR) is a novel target for promoting subcutaneous adipogenesis. *Integr Biol* 2017;9(3):223–37.
- [42] Kruszewska J, Cudnoch-Jedrzejewska A, Czarzasta K. Remodeling and fibrosis of the cardiac muscle in the course of obesity-pathogenesis and involvement of the extracellular matrix. *Int J Mol Sci* 2022;23(8).
- [43] Lewis GA, Dodd S, Clayton D, Bedson E, Eccleson H, Schelbert EB, et al. Pirfenidone in heart failure with preserved ejection fraction: a randomized phase 2 trial. *Nat Med* 2021;27(8):1477–82.
- [44] Dweck MR, Joshi S, Murigu T, Alpendurada F, Jabbour A, Melina G, et al. Midwall fibrosis is an independent predictor of mortality in patients with aortic stenosis. *J Am Coll Cardiol* 2011;58(12):1271–9.
- [45] Lopez B, Ravassa S, Gonzalez A, Zubillaga E, Bonavita C, Berges M, et al. Myocardial collagen cross-linking is associated with heart failure hospitalization in patients with hypertensive heart failure. *J Am Coll Cardiol* 2016;67(3):251–60.
- [46] Ren Z, Yu P, Li D, Li Z, Liao Y, Wang Y, et al. Single-cell reconstruction of progression trajectory reveals intervention principles in pathological cardiac hypertrophy. *Circulation* 2020;141(21):1704–19.
- [47] Eschalier R, Rossignol P, Kearney-Schwartz A, Adamopoulos C, Karatzidou K, Fay R, et al. Features of cardiac remodeling, associated with blood pressure and fibrosis biomarkers, are frequent in subjects with abdominal obesity. *Hypertension* 2014;63(4):740–6.
- [48] Weber KT, Brilla CG, Campbell SE, Zhou G, Matsubara L, Guarda E. Pathologic hypertrophy with fibrosis: the structural basis for myocardial failure. *Blood Pres* 1992;1(2):75–85.